J. Fluid Mech. (1995), *vol.* 300, *pp.* 383–407

The interaction of an isotropic field of acoustic waves with a shock wave

By KRISHNAN MAHESH, SANGSAN LEE, SANJIVA K. LELE† AND PARVIZ MOIN‡

Department of Mechanical Engineering, Stanford University, Stanford, CA 94305, USA

(Received 21 April 1994 and in revised form 26 April 1995)

Moore's (1954) inviscid linear analysis of the interaction of a shock wave with a plane acoustic wave is evaluated by comparison to computation. The analysis is then extended to study the interaction of an isotropic field of acoustic waves with a normal shock wave. The evolution of fluctuating kinetic energy, sound level and thermodynamic fluctuations across the shock wave are examined in detail.

The interaction of acoustic fluctuations with the shock is notably different from that of vortical fluctuations. The kinetic energy of the acoustic fluctuations *decreases* across the shock wave for Mach numbers between 1.25 and 1.8. For Mach numbers exceeding 3, the kinetic energy amplifies by levels that significantly exceed those found in the interaction of vortical fluctuations with the shock. Upon interacting with the shock wave, the acoustic waves generate vortical fluctuations whose contribution to the far-field kinetic energy increases with increasing Mach number. The level of sound increases across the shock wave. The rise in the sound pressure level across the shock varies from 5 to 20 dB for Mach number varying from 1.5 to 5. The fluctuations behind the shock wave are nearly isentropic for Mach number less than 1.5, beyond which the generation of entropy fluctuations becomes significant.

1. Introduction

The interaction of shock waves with a turbulent flow is a common phenomenon in a wide range of aerodynamic applications. Typical problems involving shock/turbulence interaction include the production of sound by supersonic turbulent jets, the fluctuating pressure loads on aircraft structures due to shock-induced separation and the use of a shock wave to enhance mixing. This has led to several experimental investigations, most of which examine the interaction of shock waves with boundary layers and free shear layers. The complexity of these flows has precluded isolation of the effect that the shock wave exerts. As a result, recent experiments (Debieve & Lacharme 1986; Keller & Merzkirch 1990; Honkan & Andreopoulous 1992; Jacquin, Blin & Geffroy 1991) have examined the more fundamental problem of a shock wave interacting with isotropic turbulence.

Recently, Rotman (1991), Lee, Lele & Moin (1993, 1994*a*,*b*) and Hannappel & Friedrich (1994) have numerically computed the interaction of isotropic turbulence with a normal shock. Lee *et al.* and Hannappel & Friedrich solved the three-dimensional compressible Navier–Stokes equations while Rotman solved the two-

† Also with Department of Aeronautics and Astronautics, Stanford University
‡ Also with NASA Ames Research Center

dimensional Euler equations. Rotman and Lee *et al.* compare their results to a linear theory developed by Ribner (1953, 1954, 1987) that predicts the evolution of turbulence across and downstream of the shock. The results of the DNS were seen to compare favourably with the theory.

Both Ribner and Lee *et al.* considered the interaction of solenoidal turbulence with a shock wave. However both aerodynamic flows and experimental configurations have acoustic waves in the turbulence that interacts with the shock. The influence of acoustic waves on the interaction of a turbulent flow with the shock wave is therefore a problem of fundamental importance. As the level of compressibility of a turbulent flow (parametrized by the ratio of the kinetic energy in the dilatational and solenoidal components) increases, the effects associated with the acoustic component will become important. As a prelude to this problem, we study how a field of acoustic waves interacts with a shock wave. A related problem that has received considerable attention is the propagation of a sonic boom through atmospheric turbulence. The transonic nature of that problem renders linear analysis invalid; related references may be found in the work of Crow (1969), Pierce (1971, 1992) and Rusak & Cole (1993). The focus of this paper is the influence of the dilatational component in the evolution of a turbulent flow across a shock wave. The examples outlined earlier are largely outside the transonic regime.

We extend the inviscid linear analysis of Moore (1954) to study the the interaction of an isotropic field of acoustic waves with a shock wave. Formulation of the problem and motivation for the use of linear analysis is presented in §2. A brief description and evaluation of the linear analysis is also included. The significant results of this study are presented and discussed in §3 and §4. Finally, the main conclusions are summarized in §5.

2. Linear analysis

2.1. *Background*

The linear analysis is based upon the decomposition of a compressible flow field into vorticity, acoustic and entropy modes as suggested by Kovasznay (1953). In the linear inviscid limit, these modes are decoupled from each other when the mean flow is spatially uniform. The vorticity mode has no pressure or density fluctuations but has solenoidal velocity fluctuations that are convected by the mean flow. The acoustic mode travels at the speed of sound relative to the mean flow, has isentropic pressure and density fluctuations and a corresponding irrotational velocity field that satisfies the acoustic wave equation. The entropy mode is convected by the mean flow and has no velocity or pressure fluctuations; it has only density and temperature fluctuations.

Several researchers have used linear analysis to examine the interaction of these unsteady disturbances with a shock wave. The earliest workers are apparently Blokhintzev (Landau & Lifshitz 1982), Burgers (1946) and Kantrowitz (1947), who examined the one-dimensional interaction of an acoustic wave with a normal shock wave. Carrier (1949) used linear analysis to study the stability of supersonic flow past a wedge. Interest in the configuration of shock waves in supersonic channel flow prompted Adams (1949) to study the steady interaction between a shock wave and an acoustic wave incident from upstream. Linear analysis was used by Chu (1952) to examine the interaction between a wedge-generated shock wave and an acoustic wave incident from downstream. The interaction between sound and a shock wave was also studied by Lighthill (1949). Prompted by the problem of 'shock-noise', Ribner

(1953) studied in detail the interaction between a vorticity wave and a shock wave. Ribner (1954, 1987) subsequently extended his analysis to consider a spectrum of incident vorticity waves (in three dimensions) and computed, for an isotropic incident spectrum, detailed statistics of the downstream flow field with emphasis on the generated noise. An incident spectrum of weak vortical disturbances – 'turbulence' – was seen to produce high levels of noise downstream of the shock. A detailed analysis of the unsteady interaction of an obliquely incident acoustic wave with a shock wave of infinite extent was conducted by Moore (1954). Moore studied acoustic waves that were incident from downstream as well as upstream. He also outlined extension of his analysis to study the interaction of a vorticity wave with a shock wave. Other workers that have made use of linear analysis include Kerrebrock (1956), Johnson & Laporte (1958), Lowson (1968) and McKenzie & Westphal (1968). Chang (1957) used linear analysis to examine the interaction of a plane entropy wave with an oblique shock. In addition to considering the general case of an infinite oblique shock, Chang also considered the case where the oblique shock was produced by a wedge and accounted for reflections from the wedge. Chang's theoretical results were used by Cuadra (1968) to perform a numerical parametric study of the infinite oblique shock problem.

These earlier studies were largely motivated by shock stability and the 'shock-noise' phenomenon. Recent interest in the interaction of turbulent flows with shock waves has led to renewed interest in linear analysis. Zang, Hussaini & Bushnell (1984) evaluated the linear analysis of McKenzie & Westphal (1968) by comparison to their numerical solution of the two-dimensional Euler equations. Their study, while restricted in terms of the incident angle of the disturbance, examined a wide range of shock strengths and disturbance amplitudes. Within the uncertainty of their numerical method, they concluded that linear analysis was valid over a surprisingly large range of shock strengths and disturbance amplitudes.

As mentioned earlier, Lee *et al.* (1993) conducted direct numerical simulation of the interaction of three-dimensional isotropic turbulence ($0.06 \leqslant M_t \leqslant 0.11$, where M_t is the fluctuation Mach number defined as the ratio of r.m.s. velocity to the mean speed of sound upstream of the shock wave) with a normal shock ($1.05 \leqslant M \leqslant 1.2$ where M is the mean upstream Mach number). Subsequently, stronger shock strengths ($M = 2.0, 3.0; M_t = 0.11$) were studied (Lee *et al.* 1994*b*). Detailed comparison of the DNS results to Ribner's (1954, 1987) linear analysis were made. The statistics of vorticity, turbulent kinetic energy, length scales and the fluctuating thermodynamic quantities were compared. All trends seen in the DNS were reproduced by the linear analysis, which showed good quantitative agreement for most quantities compared. An erroneous conclusion regarding the inability of the linear analysis to reproduce the rapid evolution of kinetic energy immediately downstream of the shock has been corrected (Lee *et al.* 1994*a*). Comparison of Rotman's results to linear analysis by Lee (Lele 1994) showed similar good agreement. This success of the linear analysis encourages us to use it to study the acoustic wave/shock interaction problem.

We repeat Moore's (1954) analysis of the interaction of a shock wave with a single acoustic wave that is incident from upstream. The analysis of a single wave interacting with a shock wave is evaluated by comparison to numerical computation. Integration of the results of the single acoustic wave/shock wave interaction over a spectrum of incident acoustic waves is used to describe the evolution of an isotropic field of acoustic waves across a shock wave. The observed trends are explained by appropriate decomposition of the flow field behind the shock wave. Also, differences with the interaction of isotropic vortical fluctuations with the shock wave (Ribner

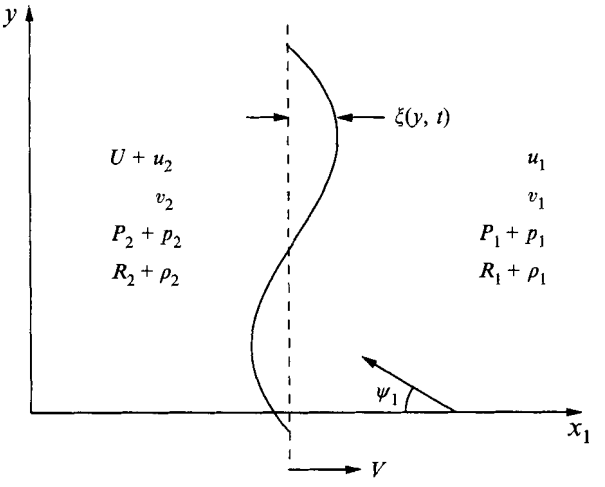

FIGURE 1. Schematic of the interaction of a shock wave with a plane acoustic wave that is incident from upstream.

1954) are discussed. Finally, the analysis is used to quantitatively describe the combined interaction of isotropic vortical and acoustic fluctuations with the shock wave.

2.2. *The interaction of a plane acoustic wave with a shock wave*

Figure 1 shows a schematic of the problem. A normal shock propagates at speed V into fluid that is at rest in the mean. The mean velocity behind the shock is denoted by U. The subscripts 1 and 2 denote the fluid in front and behind the shock respectively. The fluid at rest is assumed to be perturbed by the weak field of a plane acoustic wave that is incident at angle ψ_1 to the shock. The flow field associated with the acoustic wave is given by

$$\frac{u_1}{V} = A_1 f\left(\frac{mx_1 - ly + a_1 t}{\lambda_1}\right), \tag{1a}$$

$$\frac{v_1}{V} = A_2 f\left(\frac{mx_1 - ly + a_1 t}{\lambda_1}\right), \tag{1b}$$

$$\frac{p_1}{P_1} = A_3 f\left(\frac{mx_1 - ly + a_1 t}{\lambda_1}\right), \tag{1c}$$

$$\frac{\rho_1}{R_1} = A_4 f\left(\frac{mx_1 - ly + a_1 t}{\lambda_1}\right). \tag{1d}$$

Here, P_1, R_1 and a_1 are the mean pressure, density and sound speed in the fluid ahead of the shock while u_1 and v_1 are the disturbance velocities in the x_1- and y-directions respectively. The pressure and density fluctuations associated with the incident acoustic wave are denoted by p_1 and ρ_1. The variables l and m are related to the direction of propagation by $l = \sin\psi_1$ and $m = \cos\psi_1$ and λ_1 represents the lengthscale of the disturbance. Note that the coordinate system is fixed in the fluid that is at rest, yielding $x_1 = Vt$ at the mean position of the shock wave. The amplitudes of velocity, pressure and density are related through the governing equations for an

acoustic wave, i.e.

$$lA_1 = -mA_2; \qquad A_3 = \gamma A_4; \qquad A_1 = -\frac{m}{\gamma M}A_3. \tag{2}$$

$M = V/a_1$ is the mean Mach number of the shock wave and γ is the ratio of specific heats. Incidence of the acoustic wave causes the shock wave to deform with a profile that matches the profile of the incident wave. The linearized Rankine–Hugoniot equations are used to describe the jump of the disturbance across the disturbed shock. This yields boundary conditions for the flow behind the shock which is described by the Euler equations linearized about the uniform mean flow. The linearized Euler equations are solved in consonance with the boundary conditions to calculate the displacement of the shock wave and the flow field downstream of the shock.

The flow behind the shock wave has two distinct regimes depending upon the angle of incidence of the acoustic wave. The two regimes differ in the nature of the pressure field (and hence, its associated velocity, temperature and density field) behind the shock wave. Over a range of incident angles $0 \leqslant \psi_1 < \psi_{cl}$ or $\psi_{cu} < \psi_1 \leqslant \pi$, the pressure field behind the shock is a freely propagating plane acoustic wave. However, if $\psi_{cl} < \psi_1 < \psi_{cu}$, the pressure field behind the shock corresponds to an evanescent wave and decays exponentially. Over both these regimes, the vorticity and entropy waves propagate without decaying. ψ_{cl} and ψ_{cu} are roots of the following equation (Moore 1954):

$$\left(\frac{a_2}{V}\right)^2 - \left(1 - \frac{U}{V}\right)^2 = \left(\cot\psi_c + \frac{a_1}{V}\operatorname{cosec}\psi_c\right)^2. \tag{3}$$

Note that ψ_{cl} and ψ_{cu} depend only on the mean Mach number. The displacement of the shock front has a certain speed of propagation along the shock front due to the unsteady nature of the incident field. Analogous to the classical flexural wall problem in acoustics, (Pierce, 1981) the nature of the downstream pressure field is determined by how the speed of the disturbance along the shock front compares to the mean speed of sound and velocity downstream of the shock. Moore (1954) illustrates the two regimes geometrically. Ribner (1953) provides an equivalent explanation by noting that the unsteady interaction of an oblique wave with a normal shock can be transformed into the steady interaction of an oblique wave with an oblique shock. In the transformed coordinates, depending upon the incident angle of the wave, the flow behind the oblique shock is either supersonic or subsonic (yielding either a wave equation or Poisson equation for the pressure), which corresponds to the two regimes mentioned above.

The method for solution of the downstream flow field is given by Moore. In the interests of clarity, we reproduce his results in the Appendix. Apart from the existence of two different regimes, note that the velocity field is a linear superposition of acoustic and vortical components. Similarly, the density and temperature fields are superpositions of acoustic and entropic components. The pressure field is associated solely with the acoustic component.

2.3. *Comparison of linear analysis to numerical solution*

We compare results of the linear analysis to numerical computations of the interaction of a normal shock wave with a plane acoustic wave that is incident from upstream. The computation solves the two-dimensional compressible Navier–Stokes equations in a frame of reference that moves at the mean speed of the shock wave. The sixth-order Padé scheme (Lele 1992) is used to compute spatial derivatives and the third-order Runge–Kutta scheme (Wray 1986) is used to integrate in time. No

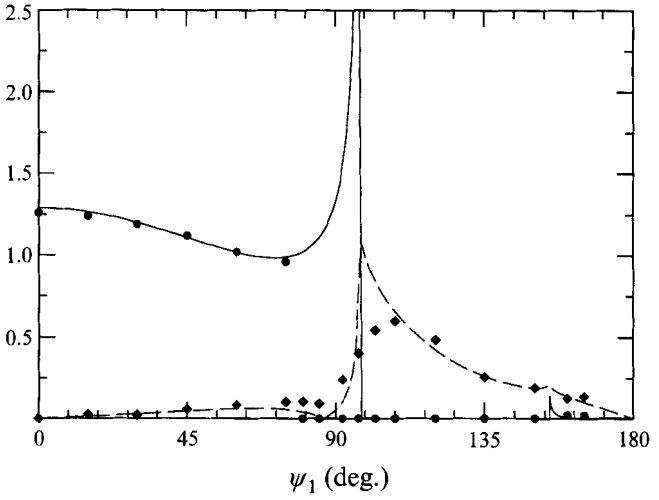

FIGURE 2. Comparison of the predictions of the linear analysis to computed results. The lines are values obtained from analysis while the symbols represent computed values. All quantities are normalized by p_1/P_1. ——, θ_2/θ_1; – – – –, ω_2/θ_1. θ_2 and ω_2 denote the r.m.s. dilatation and vorticity behind the shock wave respectively.

shock-capturing or shock-fitting is used to treat the shock wave; its structure is determined by molecular viscosity and is resolved by a non-uniform mesh (about seven points inside the shock wave).

Periodic boundary conditions are imposed at the transverse boundaries. The disturbance field corresponding to a sinusoidal acoustic wave is superposed onto the supersonic mean flow at the inflow boundary. Non-reflecting boundary conditions (Poinsot & Lele 1990) are specified at the outflow boundary. The initial condition is a numerically computed steady shock wave. The disturbance is then introduced through the inflow boundary condition. Statistics are gathered over a period of the inflow disturbance after the initial transients exit the domain.

This comparison is intended to complement that by Zang *et al.* (1984) who compared the predictions of McKenzie & Westphal's (1968) linear analysis to their numerical solution of the two-dimensional Euler equations using a shock-fitting scheme. Zang *et al.* examined the effect of incident angle, shock strength and the amplitude of the incident disturbance in the interaction of acoustic and vorticity waves with a shock wave. Results were presented only in the freely propagating regime. The dependence on incident angle was examined in the interaction of disturbances of amplitude 0.1% and 10% with a shock wave of Mach number 8. Good agreement was seen away from the critical angle; divergence from the linear analysis prediction was seen within about 20° of the critical angle. The linear analysis predictions were quite robust in terms of dependence on shock strength and disturbance amplitude. For an incident angle of 30°, the linear predictions were valid for disturbance amplitudes as high as 25% for acoustic waves and 100% for vorticity waves and shock waves whose Mach number was close to unity.

We present results of the interaction of a sinusoidal acoustic wave ($p_1/P_1 = 2.5\%$) interacting with a shock wave of Mach number 1.5. The Mach number of 1.5 was chosen to be representative of experiments on the shock/turbulence interaction. In the context of Zang *et al.*'s results, we only present the dependence on the incident angle. Results are presented in both freely propagating and decaying regimes. Figure 2

compares the computed values of r.m.s. dilatation and vorticity with predictions of the linear analysis. Note that ψ_{cl} and ψ_{cu} have values of 97.16° and 154.45° respectively for $M = 1.5$. Excellent agreement is seen except for a region within 25° of the critical angles. As noted by Zang *et al.* (for the shock wave of Mach number 8), a decaying pressure field is observed downstream of the shock wave before the critical angle is reached.

A possible reason for deviation of the computed result from the linear analysis around the critical angle is as follows. Within linear analysis, the unsteady interaction of a plane disturbance with a normal shock wave may be transformed into the *steady* interaction of the disturbance with an oblique shock wave. This transformation is an integral part of Ribner's and Chang's analysis of the interaction of a shock with a vorticity and entropy wave respectively. The transformation for the present problem involves defining coordinates x_s and y_s where

$$x_s = x - Vt; \qquad y_s = y - \frac{a_1 + mV}{l}t,$$

i.e. the flow is observed in a frame of reference that moves at the speed of the mean shock wave in the x-direction and at speed $(a_1 + mV)/l$ in the y-direction. In these transformed coordinates, the governing equations behind the shock wave are the steady Euler equations that are linearized about uniform mean flow at an equivalent Mach number that is given by the relation

$$M_e^2 = \frac{l^2(V-U)^2 + (a_1 + mV)^2}{a_2^2 l^2}.$$

This equivalent Mach number depends upon the Mach number of the normal shock wave and the incident angle of the disturbance and equals unity at the critical angle. As a result, incident angles close to the critical angle correspond to steady transonic flow downstream of the shock wave in the transformed coordinates. It is well known that the linear approximation is inconsistent in the transonic regime. We believe that the transonic small-disturbance equations are necessary to accurately represent the interaction around the critical angle.

Further indication of this is provided in figure 3, where the dependence of the interaction upon the amplitude of the incident disturbance is examined. The interaction away from the critical angle ($\psi_1 = 60°$) is compared to that close to the critical angle ($\psi_1 = 100°$). The r.m.s. intensity (p_{rms}/P) of the incident pressure fluctuation is varied from 0.14% to 14% in both cases. The vorticity (normalized by the incident dilatation) behind the shock wave is plotted against the amplitude of the incident disturbance in figure 3. The variation with the incident amplitude is negligible away from the critical angle. However, significant dependence upon the incident amplitude is seen close to the critical angle. This behaviour is in accordance with the expectation that the transonic small-disturbance equations are needed to describe the interaction around the critical angle.

2.4. *The interaction of a field of acoustic waves with a shock wave*

Moore's analysis is now extended to describe the interaction of an isotropic field of acoustic waves with the shock wave. The acoustic field is represented by a superposition of Fourier modes, each of which corresponds to a plane wave that interacts with the shock. Linearity ensures that the Fourier modes interact with the shock wave independently. Integration over time and all the incident waves is then used to describe the statistical evolution of the acoustic field across the shock.

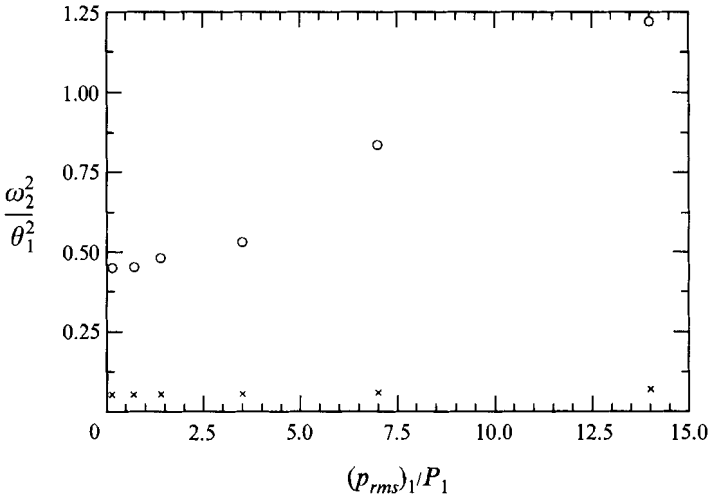

FIGURE 3. Computed values of the vorticity behind the shock wave as a function of the amplitude of the incident disturbance. The mean Mach number is 1.5. o , $\psi_1 = 100°$; × , $\psi_1 = 60°$.

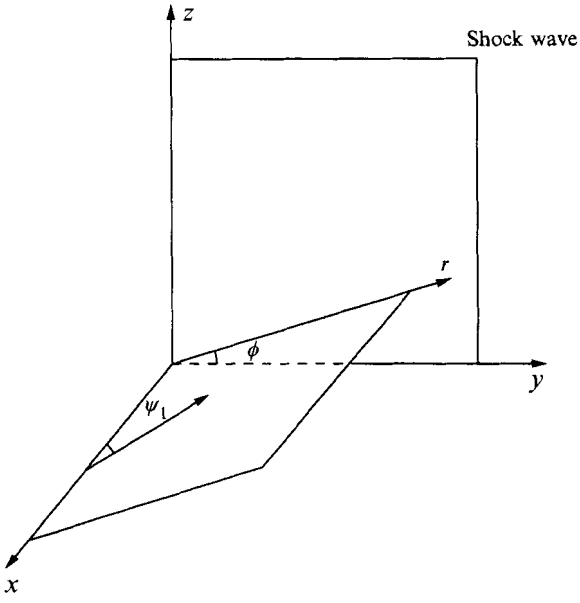

FIGURE 4. Coordinate system used in analysis of the interaction of a shock wave with an isotropic field of acoustic waves that are incident from upstream.

The use of cylindrical coordinates establishes a direct relation between Moore's two-dimensional analysis and the three-dimensional problem. Figure 4 shows a schematic of the problem in a frame of reference that moves at the speed of the undisturbed shock. The (y,z)-plane corresponds to the shock wave, while the acoustic wave lies in the (x_1,x_r)-plane that makes an angle ϕ with the y-axis. Irrotationality precludes any component of velocity outside this plane. In the (x_1,x_r)-plane, the acoustic wave makes an angle ψ_1 with the x_1-axis. It is easily seen that the (x_1,x_r)-plane is equivalent to the (x_1,y)-plane used in Moore's analysis. The incident disturbance is of the form $p_1/P_1 = A_3\ \mathrm{e}^{\mathrm{i}k(mx_1+lx_r-a_1t)}$. Comparison to equation (1c) shows that the wavenumber

$k = 1/\lambda_1$, the variables m and l retain their definitions and the coefficient A_3 is complex. Moore's two-dimensional results (see the Appendix) are therefore used in the plane of the wavenumber vector to describe the evolution of a single Fourier mode across the shock wave.

As noted in the Appendix, the solution is quite straightforward when the incident disturbance is a Fourier mode. Moore's results may be used to obtain the following expressions for the amplitude of the fluctuating field behind the shock for each incident wave. Note that we transform to a coordinate system that moves at the mean speed of the shock, i.e. our streamwise coordinate becomes $\eta_2 = -[x_2 - (V-U)t]$. Also a caret is used to indicate that the plane waves correspond to Fourier modes.

For $0 \leqslant \psi_1 < \psi_{cl}$ or $\psi_{cu} < \psi_1 \leqslant \pi$,

$$\frac{|\hat{p}_2|^2}{P_2^2} = \tilde{K}^2 \frac{|\hat{p}_1|^2}{P_1^2}, \tag{4a}$$

$$\frac{|\hat{u}_2|^2}{V^2} = \left[\tilde{F}^2 + \tilde{G}^2 + 2\tilde{F}\tilde{G}\cos\left(\frac{1}{\lambda_2}\frac{a_2}{V}\frac{\eta_2}{1-r}\right)\right]\frac{|\hat{p}_1|^2}{P_1^2}, \tag{4b}$$

$$\frac{|\hat{u}_{r2}|^2}{V^2} = \left[\tilde{H}^2 + \tilde{I}^2 + 2\tilde{H}\tilde{I}\cos\left(\frac{1}{\lambda_2}\frac{a_2}{V}\frac{\eta_2}{1-r}\right)\right]\frac{|\hat{p}_1|^2}{P_1^2}, \tag{4c}$$

$$\frac{|\hat{\rho}_2|^2}{R_2^2} = \left[\left(\frac{\tilde{K}}{\gamma}\right)^2 + \tilde{Q}^2 + 2\frac{\tilde{K}\tilde{Q}}{\gamma}\cos\left(\frac{1}{\lambda_2}\frac{a_2}{V}\frac{\eta_2}{1-r}\right)\right]\frac{|\hat{p}_1|^2}{P_1^2}. \tag{4d}$$

The constants $\tilde{K}, \tilde{F}$ and $\tilde{H}$ are associated with the acoustic component of the flow field. Similarly, $\tilde{G}$ and $\tilde{I}$ are associated with the vortical component and $\tilde{Q}$ corresponds to the entropic component.

If $\psi_{cl} < \psi_1 < \psi_{cu}$, the amplitudes behind the shock are given by

$$\frac{|\hat{p}_2|^2}{P_2^2} = \mathrm{e}^{-2d\eta_2/\lambda_1}\left[\tilde{K}_{(1)}^2 + \tilde{K}_{(2)}^2\right]\frac{|\hat{p}_1|^2}{P_1^2}, \tag{5a}$$

$$\frac{|\hat{u}_2|^2}{V^2} = \left[T_1 + T_2 + T_3\right]\frac{|\hat{p}_1|^2}{P_1^2}, \tag{5b}$$

where

$$T_1 = \tilde{G}_{(1)}^2 + \tilde{G}_{(2)}^2, \qquad T_2 = \mathrm{e}^{-2d\eta_2/\lambda_1}\left[\tilde{F}_{(1)}^2 + \tilde{F}_{(2)}^2\right],$$

$$T_3 = 2\mathrm{e}^{-d\eta_2/\lambda_1}\left[\left(\tilde{F}_{(1)}\tilde{G}_{(1)} + \tilde{F}_{(2)}\tilde{G}_{(2)}\right)\cos\delta - \left(\tilde{F}_{(2)}\tilde{G}_{(1)} - \tilde{F}_{(1)}\tilde{G}_{(2)}\right)\sin\delta\right], \quad \delta = \frac{c\eta_2}{\lambda_1}\frac{1}{1-r}.$$

The amplitude of u_{r2}/V may be obtained from the expression for u_2/V by replacing $\tilde{F}_{(1)}, \tilde{G}_{(1)}, \tilde{F}_{(2)}$ and $\tilde{G}_{(2)}$ by $\tilde{H}_{(1)}, \tilde{I}_{(1)}, \tilde{H}_{(2)}$ and $\tilde{I}_{(2)}$ respectively. The amplitude of ρ_2/R_2 may be obtained from the expression for u_2/V by replacing $\tilde{F}_{(1)}, \tilde{G}_{(1)}, \tilde{F}_{(2)}$ and $\tilde{G}_{(2)}$ by $\tilde{K}_{(1)}/\gamma, \tilde{Q}_{(1)}, \tilde{K}_{(2)}/\gamma$ and $\tilde{Q}_{(2)}$ respectively.

Analogous to the propagating regime, the constants $\tilde{K}_{(\alpha)}, \tilde{F}_{(\alpha)}$ and $\tilde{H}_{(\alpha)}$ are associated with the acoustic component of the flow field. $\tilde{G}_{(\alpha)}$ and $\tilde{I}_{(\alpha)}$ are associated with the vortical component and $\tilde{Q}_{(\alpha)}$ corresponds to the entropic component.

Components of the velocity and wavenumber vector in Cartesian coordinates are related to the those in cylindrical coordinates by the following expressions:

$$u_r = \frac{v}{\cos\phi} = \frac{w}{\sin\phi}, \quad u_\phi = 0. \tag{6a}$$

$$k_1 = k\cos\psi_1, \quad k_2 = k\sin\psi_1\cos\phi, \quad k_3 = k\sin\psi_1\sin\phi. \tag{6b}$$

Note that the solution downstream of the shock wave requires the spectrum of pressure fluctuations ahead of the shock. We assume the incident acoustic field to be isotropic. This combined with the condition of irrotationality requires the upstream spectrum of the velocity fluctuations to be of the form

$$E_{ij}(\boldsymbol{k}) = \frac{E(k)}{8\pi k^2}\frac{k_i k_j}{k^2}$$

where $E_{ij}(\boldsymbol{k})$ is the energy spectrum tensor and $E(k)$ is the three-dimensional energy spectrum. Using the acoustic relation, $A_3 = \gamma M A_1/\cos\psi_1$, and the above expression for the energy spectrum tensor, we get

$$\frac{|\hat{p}_1|^2(\boldsymbol{k})}{{P_1}^2} = \left(\frac{\gamma M}{V}\right)^2 \frac{E(k)}{4\pi k^2}. \tag{7}$$

Substituting for $|\hat{p}_1|^2(\boldsymbol{k})/{P_1}^2$ and integrating over wavenumber space at every streamwise location (η_2), we get the streamwise evolution of statistics downstream of the shock wave. Note that the elemental volume, $\mathrm{d}^3k = k^2\sin\psi_1\,\mathrm{d}\psi_1\,\mathrm{d}\phi\,\mathrm{d}k$, and $k = |\boldsymbol{k}|$ varies from 0 to ∞, ψ_1 from 0 to π and ϕ from 0 to 2π. Since the coefficients in the above equations are independent of ϕ, the integration over ϕ can be done analytically for isotropic initial spectra. For example,

$$\frac{v_2^2(\eta_2)}{V^2} = \int \cos^2\phi\,\frac{|\hat{u}_{r2}(\eta_2,k,\psi_1)|^2}{V^2}\,\mathrm{d}^3\boldsymbol{k} = \pi\int_k\int_{\psi_1}\frac{|\hat{u}_{r2}|^2}{V^2}k^2\sin\psi_1\mathrm{d}\psi_1\,\mathrm{d}k.$$

The integration over k and ψ_1 is performed numerically at every streamwise location. Note that the results depend upon the three-dimensional energy spectrum, $E(k)$. We assume the following form for $E(k)$:

$$\frac{E(k)}{V^2} \sim \left(\frac{k}{k_0}\right)^4 \mathrm{e}^{-2(k/k_0)^2}.$$

This form of the spectrum was used by Lee *et al.* (1993, 1994*b*) in their analysis of the interaction of isotropic vortical turbulence with a shock wave. There are no data that suggest the chosen spectral dependency for an isotropic field of sound waves. However, only the inhomogeneous part of the flow field behind the shock wave is dependent upon the energy spectrum of the incident waves; the far-field ($\eta_2 \to \infty$) values are *independent* of the shape of the spectrum since the integrals over k and ψ_1 separate. For example, it is easily shown that the transverse component of kinetic

energy in the far field is given by

$$\left(\frac{\overline{v_2^2}}{V^2}\right)_{\text{far field}} = \frac{\gamma M^2}{4}\left[\int_{\text{prop.}} \tilde{H}^2 + \tilde{I}^2 + \int_{\text{dec.}} \tilde{H}_{(1)}^2 + \tilde{H}_{(2)}^2\right] \sin\psi_1 d\psi_1 \int \frac{E(k)}{V^2} \mathrm{d}k.$$

The above expression uses the fact that the correlation between acoustic and vortical modes integrates to zero in the far field. Since $\int E(k)\mathrm{d}k = q_1^2/2$ the above expression is independent of the incident spectrum. We choose the same spectrum as Lee *et al.* to allow direct comparison to their results for the inhomogeneous near field behind the shock wave. Since the inhomogeneous component of the flow field exponentially decays behind the shock wave, it is the far field that is of importance and will be examined in detail.

3. Results

3.1. *Spatial variation of kinetic energy*

The evolution of the kinetic energy behind the shock wave is shown in figure 5, where $q^2 = \overline{u_2^2} + 2\overline{v_2^2}$ is plotted as a function of downstream distance. The inhomogeneous nature of the velocity field is apparent immediately downstream of the shock. Note that the curves for $M = 1.2$ and $M = 2$ are qualitatively different. While q^2 decays monotonically for $M = 1.2$, it exhibits rapid non-monotonic variation for $M = 2$. A similar rapid variation of kinetic energy was observed in the interaction of vortical fluctuations with a shock wave by Lee *et al.* (1993). However, in the shock wave/vortical turbulence interaction problem, this variation was observed at all Mach numbers considered.

Equations (5) and (6) are used to show that this variation of kinetic energy behind the shock wave is a consequence of the acoustic waves that are incident at $\psi_{cl} < \psi_1 < \psi_{cu}$. Recall that the downstream pressure field and hence the velocity field set up by these waves decayed exponentially. Equation (5*b*) shows that the downstream kinetic energy over this regime has three components: a homogeneous component associated with the vorticity waves (T_1), a monotonically decreasing component due to acoustic waves (T_2) and a non-monotonic component due to the correlation between the vorticity and acoustic waves (T_3). Upon integration over all the incident waves, these components combine to produce the rapid evolution immediately downstream of the shock. As seen from equations (5*a*) and (5*b*), the kinetic energy associated with waves incident outside this range has homogeneous vortical and acoustic components and a non-monotonic inhomogeneous component due to the correlation between them. When integrated over all incident waves, this correlation term is, however, much smaller than the other components. This is illustrated in Figure 6 where the kinetic energy is decomposed into four components (vortical, acoustic, correlation term for $\psi_{cl} < \psi_1 < \psi_{cu}$ and correlation term outside this regime) for $M = 2.0$. The correlation term associated with waves incident at $\psi_{cl} < \psi_1 < \psi_{cu}$ is seen to produce the rapid non-monotonic evolution downstream.

A similar decomposition for the $M = 1.2$ shock showed the correlation term to be insignificant resulting in the monotonic evolution of Figure 5. In our linear analysis calculations, the non-monotonic downstream variation was observed for shocks whose Mach number exceeded 1.5. In studying the interaction of vortical disturbances with the shock wave, Lee *et al.* (1993) erroneously concluded that linear analysis could not reproduce this trend which they had found in the DNS. This error was subsequently corrected and explained by them (Lee *et al.* 1994*a*,*b*).

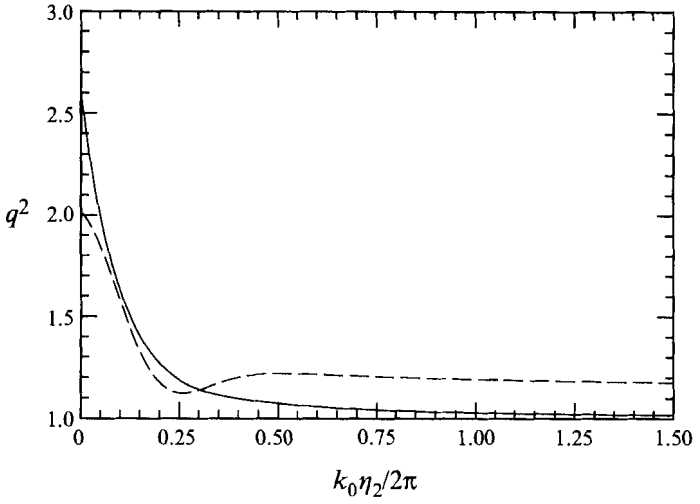

FIGURE 5. Evolution of q^2 behind the shock wave as predicted by linear analysis. q^2 is normalized with its upstream value. ——, $M = 1.2$; - - - -, $M = 2.0$.

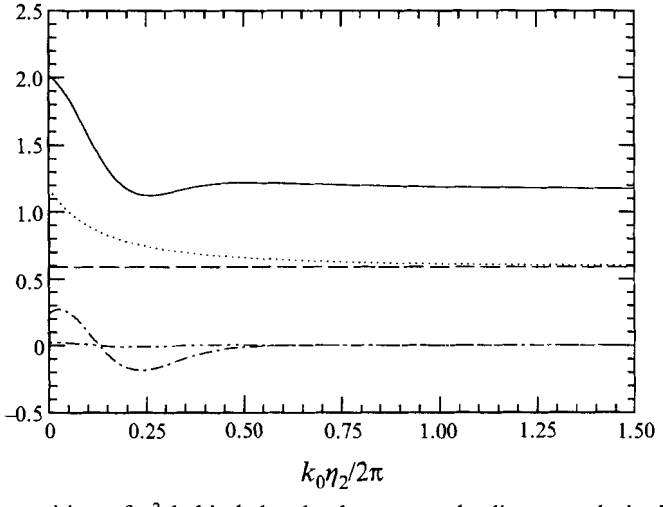

FIGURE 6. Decomposition of q^2 behind the shock wave under linear analysis. The Mach number is 2 and all components are normalized with the upstream value of q^2. ——, total; - - - -, vortical; ·····, acoustic; —·— , correlation for $\psi_{cl} < \psi_1 < \psi_{cu}$; —··— , correlation for $0 \leqslant \psi_1 < \psi_{cl}, \psi_{cu} < \psi_1 \leqslant \pi$.

The equation governing the evolution of kinetic energy downstream of the shock wave provides further insight into the spatial evolution of kinetic energy. The Euler equations linearized about uniform mean flow may be rearranged (Mahesh 1995) to show that the quantity

$$I_{\text{total}} = \frac{\gamma M}{2}\left[\frac{q^2}{a^2} + \frac{\overline{p^2}}{\gamma^2 P^2}\right] + \frac{\overline{pu}}{Pa} \tag{8}$$

is conserved along a mean streamline. I_{total} changes across the shock wave and remains unchanged downstream. The $\overline{pu}$ correlation determines the partitioning

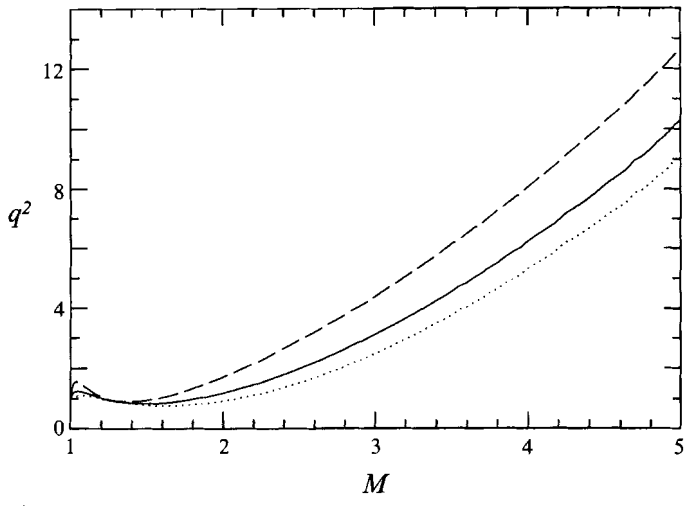

FIGURE 7. Far-field kinetic energy as a function of Mach number. All components are normalized with their upstream value. – – – –, $\overline{u^2}$; ·····, $\overline{v^2} = \overline{w^2}$; ——, q^2.

of I_{total} between potential and kinetic energy. The spatial uniformity of I_{total} and the exponential decay of $\overline{p^2}$ behind the shock wave show that the rapid evolution of q^2 behind the shock wave is a result of the rapid change in the partitioning of I_{total} through the correlation between pressure and the shock-normal component of fluctuating velocity. Decomposition of the $\overline{pu}$ correlation reveals that the rapid evolution of kinetic energy behind the shock wave is produced by the waves that are incident at $\psi_{cl} < \psi_1 < \psi_{cu}$ through the correlation between pressure and the *vortical* component of the velocity field. The far-field values of kinetic energy and pressure are, however, determined by the correlation between pressure fluctuations and the *acoustic* component of the velocity field in the *propagating* regime.

3.2. *Far-field kinetic energy*

As seen from figure 5, after a distance that is comparable to the lengthscale (taken as $2\pi/k_0$) of the incident acoustic waves, the kinetic energy asymptotes to its far-field value. The far-field values are independent of the upstream energy spectrum since the inhomogeneous terms drop out in the far field. As a result, the integration over k can be performed independently of ψ_1 and ϕ to give $\int E(k)\,\mathrm{d}k = q_1^2/2$. To gauge the effect of shock strength upon the interaction, we examine (figure 7) the far-field kinetic energy (normalized with the upstream kinetic energy) as a function of the Mach number of the shock wave. Note that the shock-normal component of kinetic energy is larger than the transverse components for all Mach numbers shown. An interesting feature of the evolution of kinetic energy is that kinetic energy *decreases* slightly across the shock wave over a range of Mach number from 1.25 to 1.80. The transverse components decrease across the shock wave over a wider range of the Mach number. This decrease in kinetic energy across the shock wave is peculiar to the acoustic wave/shock interaction problem. It is not observed in the interaction of vortical fluctuations with the shock wave where under linear analysis, kinetic energy increases across the shock wave for all shock strengths. Also, for $M > 3$, the amplification of kinetic energy is significantly higher than

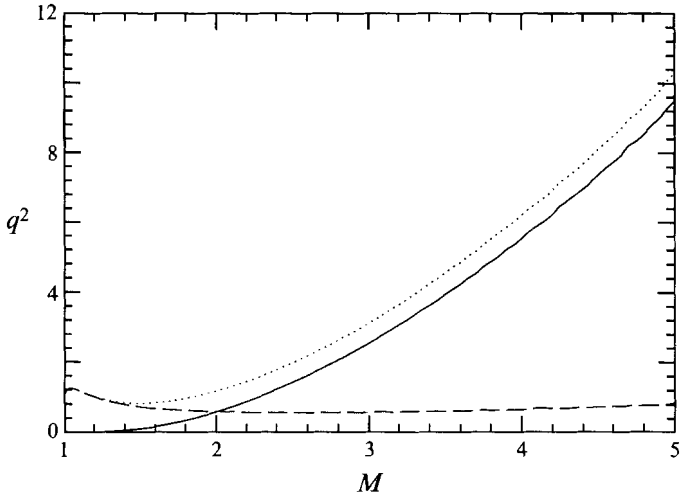

FIGURE 8. The far-field kinetic energy, decomposed into acoustic and vortical components. Both components are normalized with the upstream value of q^2. ·····, total; ——, vortical; - - - -, acoustic.

amplification levels seen in the interaction of vortical fluctuations with the shock wave.

The decrease in kinetic energy across the shock wave may be explained by decomposing (figure 8) the far field energy into acoustic and vortical components and examining their dependence on Mach number. Both components are normalized with the upstream kinetic energy. This decomposition of kinetic energy is possible since the correlation between vortical and acoustic components falls to zero in the far field. Note that the kinetic energy associated with the vortical component increases monotonically with Mach number and *exceeds* the upstream kinetic energy beyond a Mach number of about 2.25. The kinetic energy associated with the acoustic component, however, *decreases* across the shock wave for Mach numbers exceeding about 1.2. These two components compete in determining the overall evolution of kinetic energy. For lower Mach numbers, the acoustic component dominates since not enough vorticity is generated downstream, causing the overall kinetic energy to drop. At higher Mach number, the vortical component dominates due to increased generation of vortical fluctuations and the overall kinetic energy rises across the shock. The vortical component of energy exceeds the acoustic component for Mach number exceeding 2.

The decrease of the far-field acoustic kinetic energy with Mach number is explained as follows. As the Mach number increases, $\psi_{cu} - \psi_{cl}$ increases (see figure 4 of Moore) and hence a larger fraction of incident waves lie in the range $\psi_{cl} < \psi_1 < \psi_{cu}$. Recall that these waves make no contribution to the far-field acoustic kinetic energy. The only contribution to the far-field acoustic kinetic energy comes from waves incident outside this range whose amplification increases upon increasing the Mach number. Upon integrating over all incident waves, the net result of these competing factors is to produce (as seen in figure 8) a slow decrease (for $M < 3.5$) in the the far-field acoustic kinetic energy. Note that the variation of ψ_{cl} and ψ_{cu} with Mach number is most rapid at lower Mach numbers; in the limit of infinite Mach number, ψ_{cl} and

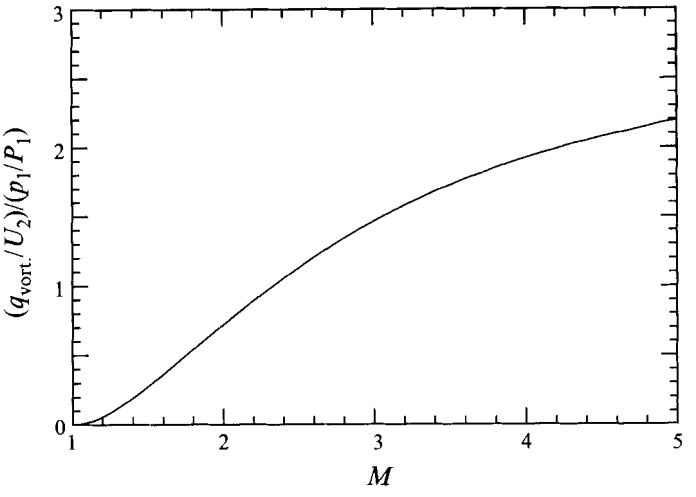

FIGURE 9. The far-field 'turbulent' intensity compared to the intensity of incident pressure fluctuations. The curve asymptotes to 2.75 ($\gamma = 1.4$).

ψ_{cu} are symmetrical about 90° and (for $\gamma = 1.4$), have values of 67.8° and 112.2° respectively.

3.3. *The production of turbulence*

Having observed the generation of vortical fluctuations – 'turbulence' – behind the shock wave, we examine in Figure 9, the intensity of the turbulence relative to the intensity of the incident pressure fluctuations. Note that $(q_{\text{vort.}}/U_2)/(p_1/P_1)$ is of the order 1 for most of the Mach numbers shown. ($U_2 = V - U$ is the mean velocity behind the shock wave if the shock were stationary in the mean.) This suggests an interesting possibility in turbulent flows involving multiple shock waves (e.g. unadapted supersonic jets). It is known that upon interaction with a shock wave, turbulence generates intense sound. For isotropic turbulence, the intensity of the sound generated, p_2/P_2, scales with the intensity of the incident turbulence q_1/U_1. In turbulent flows involving multiple shock waves, it is reasonable to expect the generated sound waves to interact with the subsequent shock waves. If this happens, figure 9 suggests that these acoustic waves can generate significant levels of turbulence through the interaction. We do not mean to suggest that our homogeneous analysis is directly applicable to flows involving shock cells, which are quite inhomogeneous. However, our results suggest that acoustic wave/shock wave interaction may be a significant generator of turbulence in these flows.

3.4. *Thermodynamic fluctuations*

Interaction with the shock wave is seen to significantly increase sound levels. Figure 10 shows the intensity (p_2/P_2) of the far-field pressure fluctuations normalized with the intensity of pressure fluctuations upstream of the shock. Note that the intensity drops, although pressure fluctuations actually amplify across the shock wave. The rise across the shock wave of the far-field sound pressure level (SPL) and the level of acoustic intensity (AIL) in dB is shown in figure 11. We define

$$\text{SPL} = 10\log\left[\frac{\overline{p^2}}{p_r{}^2}\right], \qquad \text{AIL} = 10\log\left[\frac{\overline{p^2}/\rho a}{p_r{}^2/\rho_r a_r}\right], \tag{9}$$

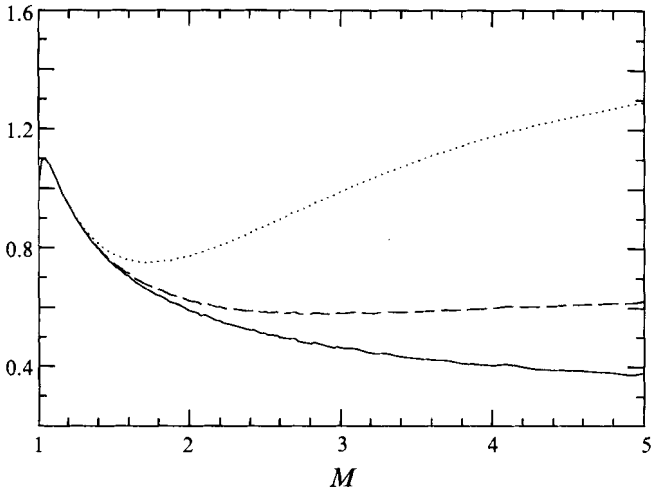

FIGURE 10. Intensity of pressure, density and temperature fluctuations in the far-field compared to the intensity of incident pressure fluctuations. ———, p_2/P_2; – – – –, $\gamma(\rho_2/R_2)$; ·····, $\gamma/(\gamma-1)(\theta_2/T_2)$. θ_2 and T_2 are the r.m.s. and mean temperature behind the shock wave respectively. The three curves are normalized with p_1/P_1 and asymptote to 0.29, 0.67 and 1.54 respectively ($\gamma = 1.4$).

where the subscript r denotes reference values. The rise in the level of sound across the shock wave is independent of the reference values. The increase in sound pressure level varies from 5 to 20 dB while the rise in acoustic intensity varies from 2 to 10 dB over the range of Mach numbers shown. Figure 10 also shows the nature of the thermodynamic fluctuations in the far field. The density and temperature fluctuations are normalized such that the three curves would collapse if the fluctuations were isentropic. We see that the isentropic relations hold until a Mach number of 1.5, beyond which the entropy fluctuations that are generated at the shock wave become significant relative to the acoustic fluctuations. The increasing importance of the entropy fluctuations in the far field is due to two factors: increased production of entropy fluctuations at the shock wave and the decrease with Mach number of the far-field intensity of pressure fluctuations. Asymptotically, $(s_2/C_p)/(p_2/P_2)$ equals 1.47 ($\gamma = 1.4$) where s_2 is the r.m.s. entropy behind the shock wave and C_p is the specific heat at constant pressure.

3.5. *Asymptotic behaviour*

Another feature that distinguishes the interaction of sound waves with a shock wave is the asymptotic behaviour with respect to Mach number. Linear analysis shows that for incident acoustic waves, quantities such as the ratio of fluctuating kinetic energy, pressure and temperature fluctuations across the shock wave are not bounded, but increase as M^2. This is easily seen from equations (5) and (6). The constants (e.g. $\tilde{K}$) in the equations have finite values in the limit of infinite Mach number and hence the intensities of velocity, density and pressure fluctuations are bounded for finite intensity of incident pressure fluctuations. However, for a given intensity of pressure fluctuations, the incident kinetic energy decreases as $1/M^2$, causing the amplification of kinetic energy to vary as M^2 for strong shocks. Similarly, since the mean pressure and temperature ratio varies as M^2 for strong shocks, the ratios of pressure and temperature fluctuations across the shock wave are not bounded. Unboundedness of kinetic energy amplification is peculiar to the acoustic wave/shock interaction

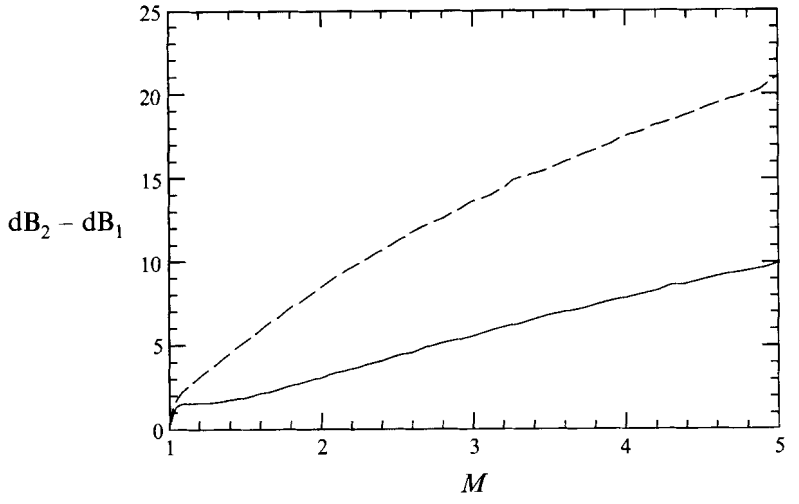

FIGURE 11. The level of far-field sound behind the shock wave compared to the incident sound level. ----, Sound pressure level; ——, level of acoustic intensity.

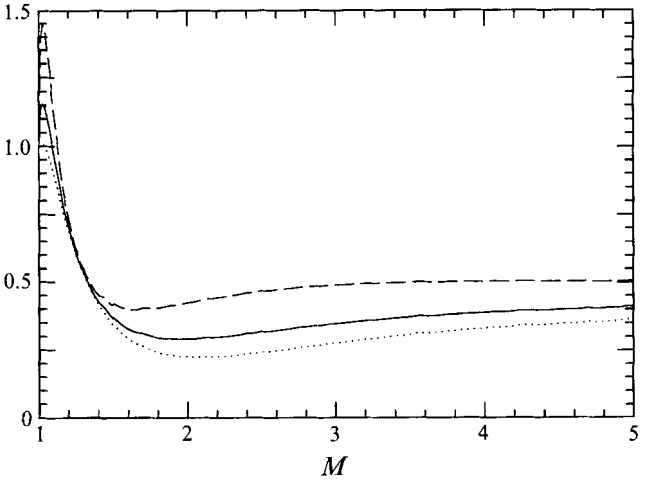

FIGURE 12. Far-field kinetic energy as a function of Mach number. All components are normalized with the incident energy and M^2. ----, $\overline{u_2^2}/M^2\,\overline{u_1^2}$; ·····, $\overline{v_2^2}/M^2\,\overline{v_1^2} = \overline{w_2^2}/M^2\,\overline{w_1^2}$; ——, $q_2^2/M^2\,q_1^2$. The three curves asymptote to 0.49, 0.40 and 0.43 respectively ($\gamma = 1.4$).

problem; it is not present when vortical fluctuations interact with the shock wave. We show in figure 12 the kinetic energy amplification normalized by M^2. Note that the amplification ratios asymptote to finite values when properly scaled with M^2.

4. Discussion

4.1. *Evaluation of linear analysis*

The inviscid linear analysis of Moore (1954) is extended to study the interaction of a three-dimensional isotropic field of acoustic waves with a normal shock wave. The objective of this study is to isolate the effect of acoustic waves on the evolution of a turbulent flow as it interacts with a shock wave. As the level of compressibility

of a turbulent flow increases, the effects associated with the acoustic component will become important. Understanding the interaction of acoustic waves with a shock wave is therefore of fundamental importance. The interaction is likely to be especially important in unbounded turbulent flows.

Our use of linear analysis is prompted by its success in past investigations. In the interaction of a single unsteady disturbance with a shock wave, there appear to be four important factors that could cause deviation from linear behaviour: proximity of the incident angle to the critical angle, the amplitude of the disturbance being non-negligible relative to the strength of the shock wave, the mean Mach number being close to unity and finally viscous effects. The linear approximation is invalid if the mean Mach number is very near unity. As mentioned before, workers such as Crow (1969), Pierce (1971, 1992) and Rusak & Cole (1993) address that regime of shock/turbulence interaction.

Proximity to the critical angle seems to be the most important factor for shocks beyond the transonic regime. Our computations of single acoustic waves interacting with a shock wave disagree with linear analysis at around 25° of the critical angle; very good agreement is seen outside this range. Fortunately, in the interaction of a spectrum of waves with a shock wave, the incident waves around the critical angle make only partial contribution to the overall energy. With regard to the amplitude of incident disturbances, results of computations are encouraging. Our computations show good agreement with linear analysis away from the critical angle for disturbance amplitudes varying from 0.14% to 14%. Zang *et al.* (1984) show that linear analysis yields good predictions away from the critical angle for acoustic disturbance amplitudes as large as 25%. Meadows, Caughey & Casper (1994) reach a similar conclusion in their study of the one-dimensional interaction of an acoustic wave with a shock wave. Their comparison of linear analysis to a nonlinear Riemann analysis yielded indistinguishable results (to plotting accuracy) for disturbance amplitudes less than 10%. An effect of increasing disturbance amplitude for a fixed shock strength has been documented by Honkan & Andreopoulous (1992) and Lee *et al.* (1992) in the interaction of isotropic turbulence with a normal shock. Both studies reported a decrease in the amplification of kinetic energy as the disturbance amplitude was increased. Honkan & Andreopoulous' experimental study had a shock of mean Mach number 1.24 while Lee *et al.*'s numerical results were for a shock wave of mean Mach number 1.2.

4.2. *Combined interaction of vortical and acoustic fluctuations*

The linearity of the analysis permits the use of superposition to predict the combined interaction of vortical and acoustic fluctuations with a shock wave. Since sound and vorticity travel at different speeds, the correlation between them can be assumed negligible upstream and in the far field behind the shock wave. The amplification of kinetic energy across the shock wave can therefore be expressed as

$$\frac{q^2}{q_0^2} = \frac{q_\omega^2 + q_\theta^2}{(q_\omega^2)_0 + (q_\theta^2)_0}, \tag{10}$$

where the subscript 0 represents conditions upstream of the shock and the subscripts ω and θ represent the vortical and dilatational components respectively. The amplification ratio in the mixed problem may be expressed in terms of the amplification ratios of vortical and acoustic fluctuations as

$$\frac{q^2}{q_0^2} = (1 - X) f_\omega + X f_\theta, \tag{11}$$

where $f_\omega = q_\omega^2/(q_\omega^2)_0$, $f_\theta = q_\theta^2/(q_\theta^2)_0$ and $X = (q_\theta^2)_0/q_0^2$. X is the ratio of acoustic to total kinetic energy upstream of the shock wave. Note that as X varies from 0 to 1, q^2/q_0^2 varies from f_ω to f_θ. Available experiments on the shock/turbulence interaction are in the range of Mach numbers for which the kinetic energy of the acoustic component decreases across the shock wave. Our results suggest that the presence of acoustic waves in these experiments will decrease the amplification of kinetic energy. As noted by Jacquin, Cambon & Blin (1993), wind-tunnel experiments on the shock/turbulence interaction report lower amplification ratios than shock-tube experiments. They suggest that boundary-layer-induced oscillation of the shock wave in the wind-tunnel experiments might be responsible (through an unknown mechanism) for this observation. Our results suggest the alternative scenario that the lower kinetic energy amplification is a consequence of acoustic waves in the turbulence ahead of the shock wave. A likely source of these sound waves are the shock waves that are generated at the edges of the grid that generates turbulence in the tunnel. Further data are needed to support or discard this scenario.

According to linear analysis (equation (11)), when compressible isentropic turbulence interacts with a shock wave, the evolution of kinetic energy lies between two limits – the pure solenoidal and pure dilatational limits. This behaviour is identical to the response of *homogenous* turbulence to one-dimensional compression. As shown by Cambon *et al.* (1993), the evolution of kinetic energy when compressible homogeneous turbulence is subjected to one-dimensional compression lies between the solenoidal and the dilatational limits. However an important difference between the shock/turbulence interaction problem and the homogeneous compression problem is the behaviour of the turbulence in the dilatational limit. For homogeneous turbulence, Cambon *et al.* show that the dilatational limit is characterized by loss of acoustic communication, which forces the pressure–strain correlation to zero, thereby yielding significantly higher amplification of q^2 as compared to solenoidal turbulence. The compressibility-induced decrease in kinetic energy across the shock wave that is seen in the acoustic wave/shock wave interaction for $1.25 < M < 1.8$ is not observed. This is due to the fundamentally different nature of the pressure fluctuations in the two problems.

The difference between the one-dimensional compression of solenoidal turbulence and Ribner's (1954, 1987) analysis of solenoidal fluctuations interacting with a shock wave was pointed out by Lee *et al.* (1993) and underscored by Jacquin *et al.* (1993). Results of the two problems agree for small Mach numbers; for large Mach numbers significantly larger amplification is seen in the homogeneous problem. Jacquin *et al.* also compare the compression of homogeneous compressible turbulence to Ribner's analysis and note that the difference between the two problems is greater than pointed out by Lee *et al.* A comparison of the compression of dilatational fluctuations to the interaction of solenoidal fluctuations with a shock wave is not appropriate; comparison should be made to the interaction of dilatational fluctuations with the shock wave. Such a comparison would reveal disagreement in the dilatational limit over the entire range of Mach numbers. While the homogeneous problem can approximate the evolution of kinetic energy in the interaction of solenoidal fluctuations with a shock wave of moderate strength, it is quite inappropriate as the incident turbulence becomes increasingly compressible.

4.3. *Comparison to computation*

Finally, we show that our analysis explains recent observations (Hannapel & Friedrich 1994) on the interaction of compressible turbulence with a normal shock. Hannapel

& Friedrich numerically computed the interaction of low Reynolds number isotropic turbulence ($R_\lambda \sim 4$ upstream of the shock wave) with a normal shock of mean Mach number 2. The fluctuating Mach number was 0.1 at the inflow and the kinetic energy was equally distributed between the vortical and acoustic modes. ($X = 0.5$ in our notation.) They compared this interaction with that of essentially solenoidal turbulence ($X = 0$) of the same fluctuating Mach number. The 'compressible' case displayed increased amplification of vorticity, decreased amplification of velocity components transverse to the shock, decreased reduction of Taylor microscale and decreased amplification of density, temperature and pressure fluctuations across the shock wave.

The computation may suffer from lack of sufficient resolution of the shock front. As a result, we do not attempt quantitative comparison. We show that the computation follows the trends predicted by the linear analysis and quote the linear analysis predictions for reference. The higher amplification of the transverse components of vorticity in the compressible case is explained by the generation of vorticity through the acoustic wave/shock wave interaction. Using an expression similar to equation (11), the increase in the amplification of vorticity may be shown to be $3g_\theta(\theta_0^2/\omega_0^2)$, where $g_\theta = \omega_2^2/\theta_0^2$ in the acoustic wave/shock wave interaction problem. Similarly, linear analysis predicts the decrease in transverse velocity and reduction in Taylor microscale. For the interaction of vortical fluctuations with a shock wave, Ribner's analysis yields $u^2/u_0^2 = 1.64$ and $v^2/v_0^2 = 1.66$ across a shock wave of Mach number 2. For dilatational fluctuations, our analysis yields values of 1.69 and 0.9 respectively. Using an expression similar to equation (11), we get $u^2/u_0^2 = 1.67$ and $v^2/v_0^2 = 1.28$, i.e. the amplification of u^2 is essentially unchanged while the amplification of the transverse velocity drops.

Linear analysis yields values of 0.53 and 0.77 for $\lambda_1/(\lambda_1)_0$ and $\lambda_2/(\lambda_2)_0$ respectively (λ_i represents the Taylor microscale in the i-direction) for the vortical problem. Corresponding values for the compressible problem are 0.66 and 0.94 respectively. The reduced amplification of thermodynamic fluctuations in the compressible problem (an order lower) is a consequence of the fact that in pure vortical turbulence, the absolute level of incident thermodynamic fluctuations is much lower (zero in the linear limit). The level of thermodynamic fluctuations behind the shock wave, however, scales with the incident kinetic energy as a result of which the amplification of thermodynamic fluctuations will be quite large (undefined within linear analysis).

5. Summary

We use inviscid linear analysis to study the evolution of fluctuating kinetic energy, sound level and thermodynamic fluctuations in the interaction of an isotropic field of acoustic waves with a normal shock wave. The analysis is an extension of Moore's (1954) study of the interaction of a shock wave with a single acoustic wave. Moore's analysis is evaluated by comparison to numerical computation. Good agreement is seen for angles away from the critical angles. A possible reason for disagreement around the critical angles is that the linear approximation is inconsistent in this regime; the transonic small-disturbance equations seem necessary.

The interaction of an isotropic acoustic field with the shock is notably different from that of vortical fluctuations. The kinetic energy of the acoustic fluctuations decreases across the shock wave for Mach numbers between 1.25 and 1.8. For Mach numbers exceeding 3, the kinetic energy amplifies by levels that significantly exceed those found in the interaction of vortical fluctuations with the shock. These trends are

explained by decomposing the velocity field into acoustic and vortical components and examining their dependence on the Mach number. Upon interacting with the shock wave, the acoustic waves generate vortical fluctuations whose contribution to the far-field kinetic energy increases with increasing Mach number. The level of sound increases across the shock wave. The rise in the sound pressure level across the shock varies from 5 to 20 dB for Mach number varying from 1.5 to 5. The fluctuations behind the shock wave are nearly isentropic for Mach number less than 1.5, beyond which the generation of entropy fluctuations becomes significant.

Finally the analysis is used to describe the combined interaction of isotropic vortical and acoustic fluctuations with a normal shock wave.

This study was supported by the Air Force Office of Scientific Research under Grant No. 88-NA-322 with Dr Leonidas Sakell as the technical monitor. The authors would also like to express their gratitude to NAS and NASA-Ames Research Center for the use of their computer facilities.

Appendix.

Moore's solution for the flow dowstream of the shock wave is given below. The subscript 2 refers to conditions behind the shock wave.

For $0 \leqslant \psi_1 < \psi_{cl}$ or $\psi_{cu} < \psi_1 \leqslant \pi$,

$$\frac{1}{A_3}\frac{p_2}{P_2} = \tilde{K} f\left(\frac{\alpha x_2 + \beta y + a_2 t}{\lambda_2}\right),$$

$$\frac{1}{A_3}\frac{\rho_2}{R_2} = \frac{\tilde{K}}{\gamma} f\left(\frac{\alpha x_2 + \beta y + a_2 t}{\lambda_2}\right) + \tilde{Q} f\left(\frac{\dfrac{m + 1/M}{1 - r} x_2 - l y}{\lambda_1}\right),$$

$$\frac{1}{A_3}\frac{u_2}{V} = \tilde{F} f\left(\frac{\alpha x_2 + \beta y + a_2 t}{\lambda_2}\right) + \tilde{G} f\left(\frac{\dfrac{m + 1/M}{1 - r} x_2 - l y}{\lambda_1}\right),$$

$$\frac{1}{A_3}\frac{v_2}{V} = \tilde{H} f\left(\frac{\alpha x_2 + \beta y + a_2 t}{\lambda_2}\right) + \tilde{I} f\left(\frac{\dfrac{m + 1/M}{1 - r} x_2 - l y}{\lambda_1}\right).$$

The x_2-axis is stationary in a frame of reference that moves with speed U yielding, $x_2 = (V - U)t$ at the mean position of the shock wave. Of the two terms that contribute to the velocity, density and temperature, the unsteady term corresponds to the acoustic wave while the steady term corresponds to the vorticity and entropy waves. The coefficients $\tilde{K}, \tilde{Q}, \tilde{G}, \tilde{H}$ and $\tilde{I}$ in the above equations are functions of the Mach number of the shock and the angle of incidence and are given below.

If $\psi_{cl} < \psi_1 < \psi_{cu}$, the solution is a bit more complex and is given by

$$\frac{1}{A_3}\frac{p_2(\eta, \xi)}{P_2} = \tilde{K}_{(1)} \Phi_{(1)}(\eta, \xi) + \tilde{K}_{(2)} \Phi_{(2)}(\eta, \xi),$$

$$\frac{1}{A_3}\frac{\rho_2}{R_2} = \frac{1}{\gamma}\frac{p_2}{P_2} + \tilde{Q}_{(1)} f\left(\frac{\dfrac{m + 1/M}{1 - r} x_2 - l y}{\lambda_1}\right) + \tilde{Q}_{(2)} g\left(\frac{\dfrac{m + 1/M}{1 - r} x_2 - l y}{\lambda_1}\right),$$

$$\frac{1}{A_3}\frac{u_2}{V} = \tilde{F}_{(1)}\Phi_{(1)}(\eta,\xi) + \tilde{F}_{(2)}\Phi_{(2)}(\eta,\xi) + \tilde{G}_{(1)}f\left(\frac{\frac{m+1/M}{1-r}x_2 - ly}{\lambda_1}\right) + \tilde{G}_{(2)}g\left(\frac{\frac{m+1/M}{1-r}x_2 - ly}{\lambda_1}\right),$$

$$\frac{1}{A_3}\frac{v_2}{V} = \tilde{H}_{(1)}\Phi_{(1)}(\eta,\xi) + \tilde{H}_{(2)}\Phi_{(2)}(\eta,\xi) + \tilde{I}_{(1)}f\left(\frac{\frac{m+1/M}{1-r}x_2 - ly}{\lambda_1}\right) + \tilde{I}_{(2)}g\left(\frac{\frac{m+1/M}{1-r}x_2 - ly}{\lambda_1}\right).$$

Analogous to the propagating regime, $\tilde{K}_{(\alpha)}, \tilde{Q}_{(\alpha)}, \tilde{G}_{(\alpha)}, \tilde{H}_{(\alpha)}$ and $\tilde{I}_{(\alpha)}$ are functions of the Mach number of the shock and the angle of incidence and are given below. Also, η and ξ are related to x_2, y and t by

$$\eta = -\frac{d}{\lambda_1}[x_2 - (V-U)t], \quad \xi = \frac{1}{\lambda_1}(\alpha x_2 + \beta y + cVt).$$

η is thus proportional to the distance behind the shock while ξ=constant represents an oblique plane moving at constant velocity. The functions $g, \Phi_{(1)}$ and $\Phi_{(2)}$ are defined as

$$g(\eta) = \frac{1}{\pi}\int_{-\infty}^{\infty}\frac{f(\tau)}{\tau-\xi}\,\mathrm{d}\tau,$$

$$\Phi_{(1)} = \frac{1}{\pi}\int_{-\infty}^{\infty} f(\tau)\frac{\eta}{\eta^2+(\tau-\eta)^2}\,\mathrm{d}\tau,$$

$$\Phi_{(2)} = \frac{1}{\pi}\int_{-\infty}^{\infty} f(\tau)\frac{\tau-\eta}{\eta^2+(\tau-\eta)^2}\,\mathrm{d}\tau.$$

Since a homogenous acoustic field may be represented as a superposition of plane waves, we consider $f(x) = \mathrm{e}^{\mathrm{i}x}$ for which $g, \Phi_{(1)}$ and $\Phi_{(2)}$ are given by

$$g(\xi) = \mathrm{i}\,\mathrm{e}^{\mathrm{i}\xi}, \quad \Phi_{(1)} = \mathrm{e}^{-\eta}\mathrm{e}^{\mathrm{i}\xi}, \quad \Phi_{(2)} = \mathrm{i}\,\mathrm{e}^{-\eta}\mathrm{e}^{\mathrm{i}\xi}.$$

Note that if the incident wave is a plane wave, the above equations take on a simple form. The coefficients in the solution are determined as follows:

$$B_1 = -\frac{2}{\gamma+1}\frac{1}{M^2}\left(1-\frac{\gamma-1}{2}M^2\right), \qquad B_2 = \left(\frac{\gamma-1}{\gamma+1}\right)\frac{2}{\gamma M^2},$$

$$C_1 = \frac{2}{1+\frac{1}{2}(\gamma-1)M^2}, \qquad C_2 = \frac{1}{\gamma}\left(1-\frac{\gamma-1}{1+\frac{1}{2}(\gamma-1)M^2}\right),$$

$$D_1 = \frac{2\gamma M^2}{\gamma M^2 - \frac{1}{2}(\gamma-1)}, \qquad D_2 = \frac{M^2-\frac{1}{2}(\gamma-1)}{\gamma M^2 - \frac{1}{2}(\gamma-1)}$$

$$l = \sin\psi_1, \quad m = \cos\psi_1, \quad n = \tan\psi_1,$$

$$r = \frac{2}{\gamma+1}\left(1-\frac{1}{M^2}\right), \qquad \left(\frac{a_2}{V}\right)^2 = (1-r)\left(1+\frac{\gamma-1}{2}r\right), \qquad \sigma = \frac{n(1-r)}{1+1/Mm}.$$

For $0 \leqslant \psi_1 < \psi_{cl}$ or $\psi_{cu} < \psi_1 \leqslant \pi$,

$$\chi = \left[1 - \frac{r(\gamma+1)(1+\sigma^2)}{2+(\gamma-1)r}\right]^{1/2},$$

$$\tilde{L} = -\frac{m}{\gamma M}\frac{\left[1+\frac{\gamma+1}{4}\frac{M}{m}\left(\frac{3-\gamma}{\gamma+1}+\frac{\gamma-1}{2}r\right)\right]\chi + \frac{\gamma+1}{4}\left[1-2\frac{\gamma-1}{\gamma+1}\frac{n}{\sigma}-\frac{n\sigma}{1-r}\right](1-r)}{1+\chi-\frac{\gamma+1}{4}r\left(1+\frac{\sigma^2}{1-r}\right)},$$

$$\tilde{K} = D_1\left(\tilde{L}+\frac{m}{\gamma M}\right)+D_2,$$

$$\tilde{Q} = C_1\left(\tilde{L}+\frac{m}{\gamma M}\right)+C_2-\frac{\tilde{K}}{\gamma},$$

$$m\frac{\lambda_2}{\lambda_1} = \frac{\frac{a_2}{V}\left(1+\frac{1}{mM}\right)}{\left(1+\frac{1}{mM}\right)^2+n^2(1-r)^2}\left[1+\left(1-r\frac{1+n^2(1-r)^2/\left(1+\frac{1}{mM}\right)^2}{1-\frac{\gamma-1}{\gamma+1}(1-r)}\right)^{1/2}\right],$$

$$\alpha = \frac{1}{1-r}\left[\frac{\lambda_2}{\lambda_1}\left(m+\frac{1}{M}\right)-\frac{a_2}{V}\right], \qquad \beta = -l\frac{\lambda_2}{\lambda_1},$$

$$\tilde{F} = -\frac{a_2}{\gamma V}\tilde{K}\alpha, \qquad \tilde{H} = -\frac{a_2}{\gamma V}\tilde{K}\beta,$$

$$\tilde{G} = \tilde{L}-\tilde{F}-B_1\left(\tilde{L}+\frac{m}{\gamma M}\right)-B_2, \qquad \tilde{I} = \frac{1+1/Mm}{n(1-r)}\tilde{G}.$$

For $\psi_{cl} \leqslant \psi_1 \leqslant \psi_{cu}$, the coefficients are as follows:

$$c = \frac{m+1/M}{1-V^2(1-r)^2/a_2^2}, \quad \alpha = -\frac{V^2}{a_2^2}(1-r)c, \quad \beta = -l, \quad d = \left(\frac{\alpha^2+l^2-V^2c^2/a_2^2}{1-V^2(1-r)^2/a_2^2}\right)^{1/2},$$

$$h_1 = -\frac{1-r}{r}\frac{1}{\sigma}\left[\frac{l}{\gamma M}+\left(\frac{m}{\gamma M}B_1+B_2\right)\frac{1}{\sigma}\right],$$

$$h_2 = 1-\frac{1-r}{r}\frac{1-B_1}{\sigma^2}, \qquad h_3 = -\frac{2d(1-r)}{l\sigma\left(1+\frac{\gamma-1}{2}r\right)},$$

$$\tilde{L}_{(1)} = \frac{h_1h_2-\left(\frac{m}{\gamma M}+\frac{D_2}{D_1}\right)h_3^2}{h_2^2+h_3^2}, \qquad \tilde{L}_{(2)} = h_3\frac{h_1+\left(\frac{m}{\gamma M}+\frac{D_2}{D_1}\right)h_2}{h_2^2+h_3^2},$$

$$h_4 = \frac{4}{\gamma+1}\frac{\sigma^2}{1+\sigma^2}, \qquad h_5 = \frac{2rd\sigma(1-r)}{l(1+\sigma^2)}\frac{V^2}{a_2^2},$$

$$\tilde{F}_{(1)} = h_4\left(\tilde{L}_{(1)}+\frac{m}{\gamma M}+\frac{D_2}{D_1}\right)-h_5\tilde{L}_{(2)}, \qquad \tilde{F}_{(2)} = h_5\left(\tilde{L}_{(1)}+\frac{m}{\gamma M}+\frac{D_2}{D_1}\right)+h_4\tilde{L}_{(2)},$$

$$\widetilde{H}_{(1)} = \frac{h_4}{\sigma}\left(\widetilde{L}_{(1)} + \frac{m}{\gamma M} + \frac{D_2}{D_1}\right) + \sigma h_5 \widetilde{L}_{(2)}, \qquad \widetilde{H}_{(2)} = -\sigma h_5\left(\widetilde{L}_{(1)} + \frac{m}{\gamma M} + \frac{D_2}{D_1}\right) + \frac{h_4}{\sigma}\widetilde{L}_{(2)},$$

$$\widetilde{K}_{(1)} = D_1\left(\widetilde{L}_{(1)} + \frac{m}{\gamma M}\right) + D_2, \qquad \widetilde{K}_{(2)} = D_1\widetilde{L}_{(2)},$$

$$\widetilde{Q}_{(1)} = C_1\left(\widetilde{L}_{(1)} + \frac{m}{\gamma M}\right) + C_2 - \frac{\widetilde{K}_{(1)}}{\gamma}, \qquad \widetilde{Q}_{(2)} = C_1\widetilde{L}_{(2)} - \frac{\widetilde{K}_{(2)}}{\gamma},$$

$$\widetilde{G}_{(1)} = \widetilde{L}_{(1)} - \widetilde{F}_{(1)} - B_1\left(\widetilde{L}_{(1)} + \frac{m}{\gamma M}\right) - B_2, \qquad \widetilde{G}_{(2)} = \widetilde{L}_{(2)}(1 - B_1) - \widetilde{F}_{(2)},$$

$$\widetilde{I}_{(1)} = \frac{1 + 1/mM}{n(1-r)}\widetilde{G}_{(1)}, \qquad \widetilde{I}_{(2)} = \frac{1 + 1/mM}{n(1-r)}\widetilde{G}_{(2)}.$$

The expression for $\widetilde{H}_{(1)}$ in Moore's paper contains a typographical error; $\widetilde{L}_{(1)} + m/\gamma M + D_2/D_1$ should be replaced by $\widetilde{L}_{(1)} + n/\gamma M + D_2/D_1$. Also, the plots of the constants when $\psi_{cl} \leqslant \psi_1 \leqslant \psi_{cu}$ do not agree with the formulae. After repeating Moore's analysis, we conclude that the formulae are correct; the figures are not.

REFERENCES

ADAMS, M. C. 1949 On shock waves in inhomogeneous flow. *J. Aero. Sci.* **16**, 685–690.

BURGERS, J. M. 1946 On the transmissions of sound waves through a shock wave. *Koninklijke Nederlandsche Akademie Van Wetenschappen, Proc.* **XLIX**, 273–281.

CAMBON, C., COLEMAN, G. N. & MANSOUR, N. N. 1993 Rapid distortion analysis and direct simulation of compressible homogeneous turbulence at finite Mach number. *J. Fluid Mech.* **257**, 641–665.

CARRIER, G. F. 1949 On the stability of the supersonic flows past a wedge. *Q. Appl. Maths* **6**, 367–378.

CHANG, C. T. 1957 Interaction of a plane shock and oblique plane disturbances with special reference to entropy waves. *J. Aero. Sci.* **24**, 675–682.

CHU, B. T. 1952 On weak interaction of strong shock and Mach waves generated downstream of a shock. *J. Aero. Sci.* **19**, 433–446.

CROW, S. C. 1969 Distortion of sonic bangs by atmospheric turbulence. *J. Fluid Mech.* **37**, 529–563.

CUADRA, E. 1968 Flow perturbations generated by a shock wave interacting with an entropy wave. *AFOSR-UTIAS Symp. on Aerodynamic Noise, Toronto*, pp. 251–271.

DEBIEVE, J. F. & LACHARME, J. P. 1986 A shock wave/free-turbulence interaction. In *Turbulent Shear Layer/Shock Wave Interactions* (ed. J. Délery). Springer.

HANNAPPEL, R. & FRIEDRICH, R. 1994 DNS of a M=2 shock interacting with isotropic turbulence. In *Proc. First ERCOFTAC Workshop on DNS and LES, Guildford, Surrey, UK.*

HONKAN, A. & ANDREOPOULOUS, J. 1992 Rapid compression of grid-generated turbulence by a moving shock wave. *Phys. Fluids* A **4**, 2562–2572.

JACQUIN, L., BLIN, E. & GEFFROY, P. 1991 Experiments on free turbulence/shock wave interaction. In *Proc. Eighth Symp. on Turbulent Shear Flows, Munich* (ed. F. Durst, R. Friedrich, B. E. Launder, F. W. Schmidt, U. Schumann & J. H. Whitelaw). Springer.

JACQUIN, L., CAMBON, C. & BLIN, E. 1993 Turbulence amplification by a shock wave and rapid distortion theory. *Phys. Fluids* A **5**, 2539–2550.

JOHNSON, W. R. & LAPORTE, O. 1958 Interaction of cylindrical sound waves with a stationary shock wave. *Phys. Fluids* **1**, 82–94.

KANTROWITZ, A. 1947 The formation and stability of normal shock waves in channel flow. *NACA TN* 1225.

KELLER, J. & MERZKIRCH, W. 1990 Interaction of a normal shock wave with a compressible turbulent flow. *Exps. Fluids* **8**, 241–248.

KERREBROCK, J. L. 1956 The interaction of flow discontinuities with small disturbances in a compressible fluid. PhD thesis, California Institute of Technology.

KOVASZNAY, L. S. G. 1953 Turbulence in supersonic flow. *J. Aero. Sci.* **20**, 657–682.

LANDAU, L. D. & LIFSHITZ, E. M. 1982 Fluid Mechanics. *Course of Theoretical Physics*, Vol. 6, pp. 332-333. Pergamon Press.

LEE, S., LELE, S. K. & MOIN, P. 1993 Direct numerical simulation of isotropic turbulence interacting with a weak shock wave. *J. Fluid Mech.* **251**, 533–562.

LEE, S. LELE, S. K. & MOIN, P. 1994*a* Corrigendum to **251**, 1993, 533–562. *J. Fluid Mech.* **264**, 373–374.

LEE, S. LELE, S. K. & MOIN, P. 1994*b* Interaction of isotropic turbulence with a strong shock wave. *AIAA Paper* 94-0311.

LELE, S. K. 1992 Compact finite difference schemes with spectral-like resolution. *J. Comput. Phys.* **103**, 16–42.

LELE, S. K. 1994 Compressibility effects on turbulence. *Ann. Rev. Fluid Mech.* **26**, 211–254.

LIGHTHILL, M. J. 1949 The flow behind a stationary shock. *Phil. Mag.* (7) 40, 214–220.

LOWSON, M. V. 1968 Pressure fluctuations resulting from shock interactions. *J. Sound Vib.* **7**, 380–392.

MAHESH, K. 1995 The interaction of a shock wave with a turbulent shear flow. PhD thesis, Dept of Mechanical Engineering, Stanford University.

MCKENZIE, J. F. & WESTPHAL, K. O. 1968 Interaction of linear waves with oblique shock waves. *Phys. Fluids* **11**, 2350–2362.

MEADOWS, K. R., CAUGHEY, D. A. & CASPER, J. 1993 Computing unsteady shock waves for aeroacoustic applications. *AIAA Paper* 93-4329.

MOORE, F. K. 1954 Unsteady oblique interaction of a shock wave with a plane disturbance. *NACA TN* 2879.

PIERCE, A. D. 1971 Statistical theory of atmospheric turbulence effects on sonic-boom rise times. *J. Acoust. Soc. Am.* **49**, 906–924.

PIERCE, A. D. 1981 *Acoustics: An Introduction to its Physical Principles and Applications.* McGraw-Hill.

PIERCE, A. D. 1992 Wave equations and computational models for sonic boom propagation through a turbulent atmosphere. *NASA CP* 3172.

POINSOT, T. J. & LELE, S. K. 1990 Boundary conditions for direct simulation of compressible viscous reacting flow. *Center for Turbulence Research Manuscript* 102. Stanford University/NASA Ames.

RIBNER, H. S. 1953 Convection of a pattern of vorticity through a shock wave. *NACA TN* 2864.

RIBNER, H. S. 1954 Shock-turbulence interaction and the generation of noise. *NACA TN* 3255.

RIBNER, H. S. 1987 Spectra of noise and amplified turbulence emanating from shock-turbulence interaction. *AIAA J.* **25**, 436–442.

ROTMAN, D. 1991 Shock wave effects on a turbulent flow. *Phys. Fluids* A **3**, 1792–1806.

RUSAK, Z. & COLE, J. D. 1993 Interaction of the sonic boom with atmospheric turbulence. *AIAA Paper* 93-2943.

WRAY, A. A. 1986 Very low storage time-advancement schemes. *Internal Rep.* NASA-Ames Research Center.

ZANG, T. A., HUSSAINI, M. Y. & BUSHNELL, D. M. 1984 Numerical computations of turbulence amplification in shock-wave interactions. *AIAA J.* **22**, 13–21.